

Molecular dynamics study of the initial stages of catalyzed single-wall carbon nanotubes growth: force field development

Alberto Martinez-Limia · Jin Zhao · Perla B. Balbuena

Received: 27 October 2006 / Accepted: 14 February 2007 / Published online: 9 March 2007
© Springer-Verlag 2007

Abstract Effective force fields for Ni-C interactions developed by Yamaguchi and Maruyama for the formation of metallofullerenes are modified to simulate the catalyzed growth of single-wall carbon nanotubes on Ni_n clusters with $n > 20$, and the reactive empirical bond order Brenner potential for C-C interactions is also revised to include the effect of the metal atoms on such interactions.

Keywords Molecular dynamics · Reactive force field · Density functional theory · Carbon nanotubes · Catalytic growth

Introduction

Carbon nanotubes, and particularly single-walled nanotubes (SWNTs) [1], are currently grown using several techniques like laser ablation, [2] arc discharge, [3] and chemical vapor deposition [4–7]. In the first two cases, nanotubes are obtained after condensation of hot carbon gas, while in the latter case the growth is determined by the presence of a catalyst (usually based on transition metals like Ni, Co, or Fe), which causes the separation of the carbon present in

the precursor gas (example CO, C_2H_2 , CH_4) and assists as seed-site for the nanotube growth. Lately, researchers have successfully produced SWNTs with diameter and chirality selectivity, which makes them extremely attractive for several technological applications [8, 9]. However, some aspects of the nanotube growth and selectivity mechanisms are still debated.

Theoretical studies, particularly classical and quantum molecular dynamics simulations, are powerful tools to investigate the growth mechanism [10–23] because they offer the possibility of analyzing the growth process with controlled parameters, such as size and structure of the analyzed catalytic nanoparticles, at low cost, providing detailed information, and guiding experimental studies for further characterization. It is expected that computational studies may help to develop a better understanding of the SWNT growth process, making it possible to learn about the role of the nanoparticles in determining the nanotube structures.

Carbon-carbon interactions have been successfully modeled using the reactive empirical bond order (REBO) Brenner potential [24, 25]. Based on density functional calculations of small clusters NiC_n and Ni_n ($n=1 \sim 3$), metal-C and metal-metal reactive force fields have been developed to simulate catalytic growth of nanotubes and fullerene [16, 17, 26, 27], where the catalysts consist of a few metal atoms. In this work, we have adapted the Ni-C potential functions proposed by Yamaguchi and Maruyama [27] and the Brenner C-C potential [25], in order to model the main features of the catalyzed SWNT synthesis process. Results from classical molecular dynamics simulations of the initial stages of SWNT's catalyzed growth using the modified potentials have been reported elsewhere [21, 22].

A. Martinez-Limia · J. Zhao · P. B. Balbuena (✉)
Department of Chemical Engineering, Texas A&M University,
College Station, TX 77843, USA
e-mail: balbuena@tamu.edu

A. Martinez-Limia
Chemnitz University of Technology,
Institute of Electrical and Information Engineering,
09126 Chemnitz, Germany

Force fields

Main interatomic interactions present in a SWNTs catalyzed growth process

Since the focus of this work is to develop the mathematical functions able to describe the metal-C and C-C interactions in a catalyzed synthesis of SWNTs, we first provide some details of what is known about the process from theoretical and experimental investigations. As mentioned in the introduction, one successful synthesis method is based on chemical vapor deposition of a precursor gas on an appropriate catalytic surface, at pressures that vary between a few atm [8] and ~80–100 atm [5] and temperatures in the order of ~1,000–1,300 K. The catalyst is usually a nanoparticle (from 0.5 to a few nanometers size) of a transition metal (Co, Fe, Ni, and others) that could be floating in a vapor [2] or supported on a substrate [28].

A synthesis process using CO as C-containing precursor gas may be summarized in a few steps: (1) decomposition of the precursor gas on the surface of the catalyst ($2\text{CO} \Rightarrow \text{C} + \text{CO}_2$), leading to C deposition and production of CO_2 gas that is removed from the system; (2) diffusion of the C atoms to the interior of the nanoparticle until the nanoparticle is saturated (the carbon concentration limit could be given by carbon solubility in the metal nanoparticle, although rigidity of the nanocatalyst due to a strong interaction with its substrate may cause variations in this limit, see, for example, reference [22]); (3) C atoms precipitate on the surface and start forming chains; (4) chains combine to form rings and fullerene-type networks; (5) a nanotube cap may be formed that lifts off the catalyst surface; and (6) the cap grows evolving into the nanotube.

Thus, the main interatomic interactions present in this system are: metal-metal interactions in the nanocatalyst particle, metal-C interactions inside the catalyst, metal-C interactions on the surface of the catalyst, C-C interactions inside the metal nanoparticle, C-C interactions on the surface of the metal nanoparticle, and C-C interactions in the carbon nanostructure (cap or nanotube) sufficiently far from the metal atoms. With the exception of the metal-metal interactions, we consider all the above interatomic forces in the following section to develop appropriate force fields needed to describe the bond breaking and bond forming processes in the synthesis of SWNTs.

Metal-carbon potential

Yamaguchi and Maruyama [27] introduced many-body potential functions (Eqs. (1–3)) to describe the interaction between metal and C atoms, where E_b , the interaction energy between two atoms i and j separated a distance r_{ij} , is

computed as the combination of Morse-type repulsive and attractive terms, $V^R(r_{ij})$ and $V^A(r_{ij})$, respectively,

$$E_b = V^R(r_{ij}) - V^A(r_{ij}) \quad (1)$$

$$V^R(r_{ij}) = f(r_{ij}) \frac{D_e}{S-1} \exp \left\{ -\beta \sqrt{2S} (r_{ij} - R_e) \right\} \quad (2)$$

$$V^A(r_{ij}) = f(r_{ij}) \frac{D_e S}{S-1} \exp \left\{ -\beta \sqrt{2/S} (r_{ij} - R_e) \right\} \quad (3)$$

$f(r)$ is a cutoff function for the potential, given by:

$$f(r) = \begin{cases} 1 & (r < R_1) \\ \left(1 + \cos \left(\pi \frac{r-R_1}{R_2-R_1} \right) \right) / 2 & (R_1 < r < R_2) \\ 0 & (r > R_2) \end{cases} \quad (4)$$

$f(r)$ is also used to determine the coordination number N_i^M of the atom i , and R_1 and R_2 are model parameters, as explained later. D_e and R_e are the equilibrium binding energy and bond distance between i and j , calculated as functions of an average atomic coordination number N_{ij} ,

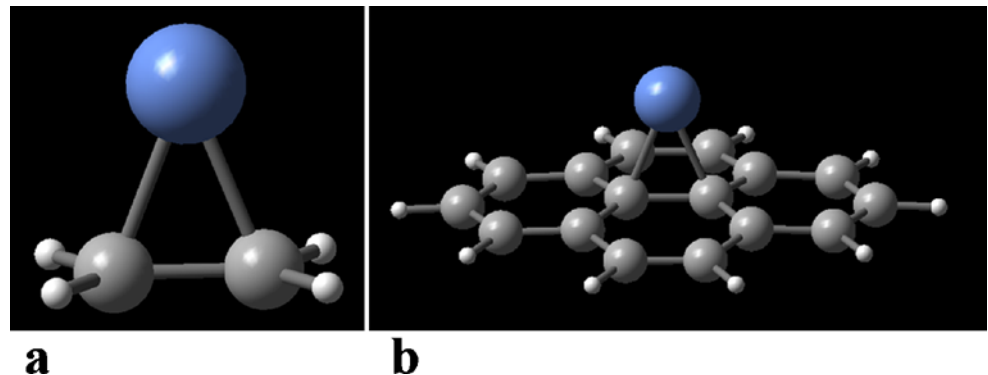
$$D_e = D_{e1} + D_{e2} \exp [-C_D(N_{ij})] \quad (5)$$

$$R_e = R_{e1} - R_{e2} \exp [-C_R(N_{ij})] \quad (6)$$

S and β in Eqs. (2) and (3), are parameters taken from the original reference [27]. Estimation of D_{e1} , D_{e2} , C_D , C_R , R_{e1} , and R_{e2} for the Ni-C system is discussed at the end of this section.

In clusters of more than 20 atoms it is possible that one carbon is bonded to 3 (when C is on the surface of the metal cluster) or even up to 8 metal atoms (when C is inside of the cluster). To account for these interactions, our modified potential includes the dependence that arises from the presence of several metal atoms around a carbon atom j . In addition, the effect of different bonding structures such as fullerene and carbon chains interacting with metal atoms are also added to the potential function that describes carbon-metal interactions. Two systems (NiC_2H_4 and $\text{NiC}_{16}\text{H}_{10}$) were investigated to establish possible differences in the metal-carbon bond of carbon atoms which are also involved in sp^2 or sp^3 carbon-carbon bonds. DFT optimizations at the B3PW91/LANL2DZ level of NiC_2H_4 and $\text{NiC}_{16}\text{H}_{10}$ (Fig. 1) provided an estimate for the total C-Ni binding energy of 0.64 and 0.12 eV, respectively. This is a remarkable difference compared to the 4.2 eV of binding energy for a single C atom bonded to three metal atoms—the most common case on the surface of a metal cluster.

Fig. 1 Optimized geometries of NiC_2H_4 and $\text{NiC}_{16}\text{H}_{10}$



Similar estimations have been made by other authors [29], and led us to assume that the C atoms bonded in graphite-type structures are weakly bonded to the metal surface. To describe this feature, Eq. (1) is modified so that the energy of the bond between the metal atom i and the carbon atom j is described by the potential function:

$$E_{ij}^{MC} = G\left(\alpha_{ij}^{MC}, V^R(r_{ij}), V^A(r_{ij})\right) \quad (7)$$

where a new parameter α_{ij}^{MC} (Eq. (12)), which is a function of the bonding status of carbon atom j , is introduced in the metal-C potential. α_{ij}^{MC} equals 1 when the carbon atom j does not bond to other carbon atoms (C0); α_{ij}^{MC} equal to α_1^{MC} , a value between 0 and 1, when the carbon atom j is bonded to two other C atoms (CII), and when the carbon atom j is bonded to three other C atoms (CIII), α_{ij}^{MC} equals a value α_2^{MC} , which is still greater than 0, but smaller than α_1^{MC} .

The function G in Eq. (7) is designed to modify the attractive and repulsive parts of the potential using varying values of the α_{ij}^{MC} parameter, in the interval $0 < \alpha_{ij}^{MC} < 1$. Such behavior is needed for the description of C-metal interactions in cases when a C atom is bonded to other C atoms and therefore weakly bonded to the metal, while a repulsive core remains in place. The most successful form of $G\left(\alpha_{ij}^{MC}, V^R(r_{ij}), V^A(r_{ij})\right)$ is given by:

$$G = \alpha_{ij}^{MC} V^R(r_{ij}) - \left(\alpha_{ij}^{MC}\right)^{1.1} V^A(r_{ij}) \quad (8)$$

To include the effect of several metal atoms surrounding a carbon atom j , instead of defining a repulsive and attractive part as function of *carbon* coordination number as in Yamaguchi and Maruyama potential [27], we define them as a function of N_{ij} , which is a *total* coordination number including the relative influence of the carbon and metal coordination numbers N_i^C and N_j^M as shown in Eqs. (9–11).

$$N_i^C = \sum_{\text{carbon } k \neq i} f(r_{ik}) \quad (9)$$

$$N_j^M = \sum_{\text{metal } k \neq j} f(r_{jk}) \quad (10)$$

$$N_{ij} = N_j^M + \lambda N_i^C \quad (11)$$

The λ parameter weights the contribution of the metal and C coordination numbers.

$$\alpha_{ij}^{MC} = \begin{cases} 1 & (N_{\text{carbon}}^C < N_i^C, \text{i.e. } C(0)) \\ \alpha_1^{MC} + \frac{(1-\alpha_1^{MC})}{2} \left[1 + \cos \left(\pi \frac{N_{\text{carbon}}^C - N_1^C}{N_2^C - N_1^C} \right) \right] & (N_1^C < N_{\text{carbon}}^C < N_2^C) \\ \alpha_1^{MC} & (N_2^C < N_{\text{carbon}}^C < N_3^C, \text{i.e. } C(II)) \\ \alpha_2^{MC} + \frac{(\alpha_1^{MC} - \alpha_2^{MC})}{2} \left[1 + \cos \left(\pi \frac{N_{\text{carbon}}^C - N_3^C}{N_4^C - N_3^C} \right) \right] & (N_3^C < N_{\text{carbon}}^C < N_4^C) \\ \alpha_2^{MC} & (N_{\text{carbon}}^C > N_4^C, \text{i.e. } C(III)) \end{cases} \quad (12)$$

Other $G\left(\alpha_{ij}^{MC}, V^R(r_{ij}), V^A(r_{ij})\right)$ functions were tested, with less satisfying results, for example Eq. (13) where the metal-C potential is reduced by $0.0 < \alpha_{ij}^{MC} < 1.0$, while the function $V^{LJ}(r_{ij})$ maintains the necessary repulsive core.

$$G = \alpha_{ij}^{MC} (V^R(r_{ij}) - V^A(r_{ij})) + (1.0 - \alpha_{ij}^{MC}) V^{LJ}(r_{ij}) \quad (13)$$

with

$$V^{LJ}(r_{ij}) = 4\varepsilon \left[\left(\frac{\sigma}{r_{ij}} \right)^{12} - \left(\frac{\sigma}{r_{ij}} \right)^6 \right] \quad (14)$$

An alternative form of G where the attractive part is reduced and the repulsive part remains intact was also tested:

$$G = V^R(r_{ij}) - \alpha_{ij}^{MC} V^A(r_{ij}) \quad (15)$$

Analysis of G from Eqs. (13) and (15) shows that the dimension of their repulsive cores could change very rapidly as a function of time (because α_{ij}^{MC} depends on the position of atoms that are not directly involved on the given bond), thus requiring the use a very short simulation step (less than 0.1 fs) to avoid instabilities because of strong repulsive forces that can appear from one time step to the next one. Figure 2 shows the effect of α_{ij}^{MC} on the function G (Eq. (8))

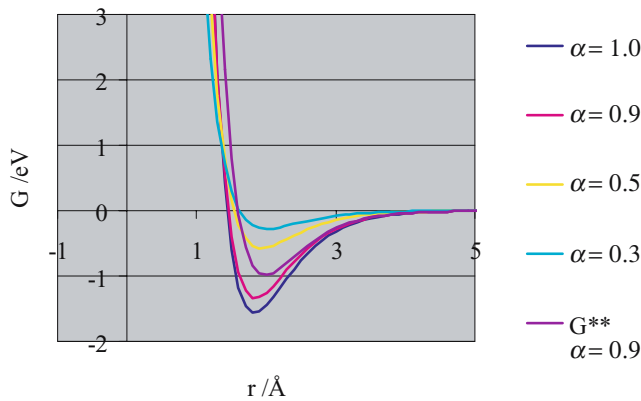


Fig. 2 Behavior of the G function (Eq. (8)) for different values of α_{ij}^{MC} . For comparison, the potential for Eq. (15) (denoted as G^{**}) is shown for $\alpha_{ij}^{MC} = 0.9$, where a drastic change of the size of the repulsion core is observed

suggesting that changing α_{ij}^{MC} in a wide range maintains the size of the repulsive core almost intact. Equation (8) satisfies the requirement that the repulsive core does not change with α_{ij}^{MC} .

Another requirement for the G function is that it should yield the correct potential shape to account for the case of carbon chains and for carbon bonded to three other carbon atoms. Figure 3 shows the potential functions (8) and (16) for α_{ij}^{MC} values of 1, 0.85, and 0.15 corresponding to the cases where the carbon atom j is not bonded to any other carbon atoms, when is bonded to two other carbons, and when is bonded to three other carbon atoms, respectively.

$$G = \left(\alpha_{ij}^{MC}\right)^{0.8} V^R(r_{ij}) - \left(\alpha_{ij}^{MC}\right)^{1.1} V^A(r_{ij}) \quad (16)$$

At the beginning of the simulation, these functions perform correctly. But after the metal cluster is covered by many carbon chains, these chains do not combine to form fullerene structures as described in the previous section when Eq. (16) is used, but they do with Eq. (8). This difference in behavior of the two functions comes from the different equilibrium bond distance of the metal-C bond (the position corresponding to the bottom of the potential well in Fig. 3) when a carbon atom is bonded to three other carbon atoms. As seen in Fig. 3, when α_{ij}^{MC} equals 0.85, the equilibrium bond lengths are about 1.8 Å for both functions. But when α_{ij}^{MC} equals 0.15, with Eq. (8) the equilibrium bond length is about 2 Å which is very close to the bond length of 1.95 Å found in the calculated NiC₁₆H₁₀ cluster, while with Eq. (16), it is about 2.4 Å.

The potential parameters shown in Table 1 were adjusted using Eqs. (5) and (6) to fit DFT results (Fig. 4) of several clusters of Ni_n and CNi_n ($n=1\text{--}4, 6, 8$) with high symmetry; the calculated and fitted results are shown in Fig. 4.

Carbon-carbon potential

For the modeling of the interaction among carbon atoms we start from the reactive empirical bond order (REBO) potential developed by Brenner et al. [25], which is based on the Tersoff [30] and Tersoff-Brenner potentials [24]. Carbon-carbon interactions have been successfully modeled using this potential, defined by a potential function between the C atoms i and j , that includes repulsive and attractive terms V^R and V^A . In our model, we define the C-C energy introducing a function $G(\alpha_{ij}^{TB}, V_{ij}^{TB})$ in order to obtain a better description of some particular C-C interactions during the SWNT growth process in a similar manner as done for the carbon-metal potential.

$$E_{ij}^{CC} = G(\alpha_{ij}^{TB}, V_{ij}^{TB}) \quad (17)$$

$$V_{ij}^{TB} = V^R(r_{ij}) - V^A(r_{ij}) \quad (18)$$

$$V^R(r) = f^c(r) \left(1 + Q/r\right) A e^{-ar} \quad (19)$$

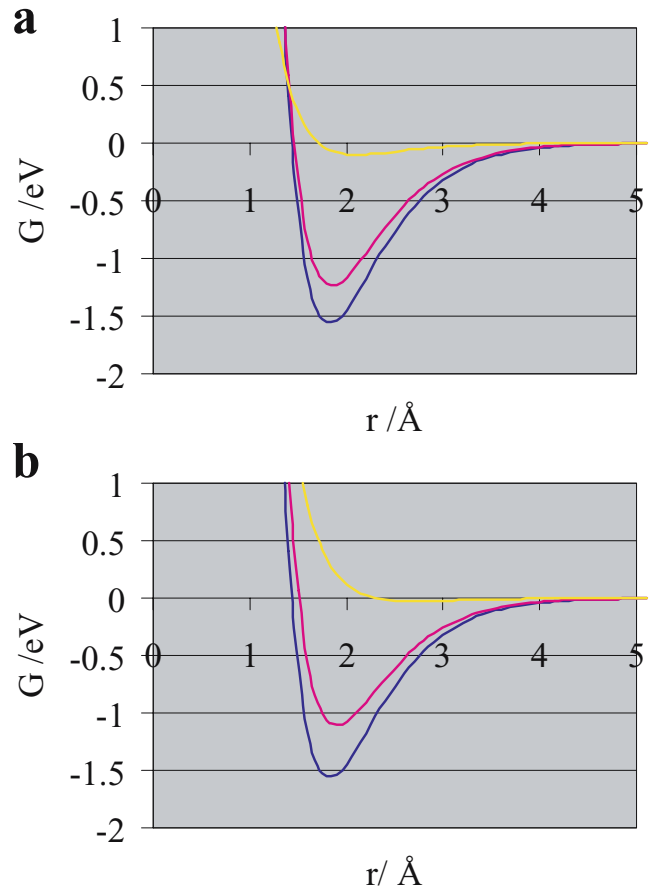


Fig. 3 Behavior of the G function for values of α_{ij}^{MC} equal 1 (purple line), 0.85 (red line) and 0.15 (black line). **a**) Eq. (8); **b**) Eq. (16)

Table 1 Parameters for Ni-C potential

β (1/Å)	D_{e1} (eV)	D_{e2} (eV)	C_D	R_{e1} (Å)	R_{e2} (Å)	C_R	R_1 (Å)	R_2 (Å)	S
1.8	0.95	1.65	0.5	1.9	0.2	0.5	2.7	3.0	1.3
λ	N_1^C	N_2^C	N_3^C	N_4^C	α_1^{MC}	α_2^{MC}			
0.08	~1.5	2.0	~2.5	3.0	~0.8	~0.15			

$$V^A(r) = b_{ij} \left(f^c(r) \sum_{n=1,3} B_n e^{-\beta_n r} \right) \quad (20)$$

where b_{ij} is an empirical bond order function that depends on the local coordination and bond angles of atoms i and j .

The weighting factor α_{ij}^{TB} is defined in Eqs. (21–28)

$$\alpha_{ij}^{TB} = \sqrt{\alpha_{1ij}^{TB} \alpha_{2ij}^{TB}} \quad (21)$$

$$\alpha_{1ij}^{TB} = \begin{cases} 1 & \left(N_{ij}^M < N_i^M \right) \\ \left(1 + \cos \left(\pi \frac{N_{ij}^M - N_i^M}{N_2^M - N_1^M} \right) \right) / 2 & \left(N_i^M < N_{ij}^M < N_2^M \right) \\ 0.1 & \left(N_{ij}^M > N_2^M \right) \end{cases} \quad (22)$$

$$N_{ij}^M = \frac{N_i^M + N_j^M}{2.0} \quad (23)$$

$$N_i^M = \sum_{\text{metal } k} f(r_{ik}) \quad (24)$$

$$N_j^M = \sum_{\text{metal } k} f(r_{jk}) \quad (25)$$

$$f(r) = \begin{cases} 1 & (r < R_1) \\ \left(1 + \cos \left(\pi \frac{r-R_1}{R_2-R_1} \right) \right) / 2 & (R_1 < r < R_2) \\ 0 & (r > R_2) \end{cases} \quad (26)$$

$$\alpha_{2ij}^{TB} = \sqrt{\alpha_{2i}^{TB} \alpha_{2j}^{TB}} \quad (27)$$

$$\alpha_{2i}^{TB} = \begin{cases} 1 & \left(R_i^M < R_1^M \right) \\ \left(1 + \cos \left(\pi \frac{R_i^M - R_1^M}{R_2^M - R_1^M} \right) \right) / 2 & \left(R_1^M < R_i^M < R_2^M \right) \\ 0.1 & \left(R_i^M > R_2^M \right) \end{cases} \quad (28)$$

The resulting α_{ij}^{TB} is obtained using the combination rule of Eq. (21) from the two factors α_{1ij}^{TB} and α_{2ij}^{TB} . α_{1ij}^{TB} describes the fact that the bonding energy between two C atoms inside of the metal cluster is very weak (between 0.05 eV and 0.10 eV [31] or even repulsive), our DFT results on C_2Ni_3 gave a binding energy of 0.44 eV. For comparison, the C-C bonding energy according to the original REBO potential is about 6.3 eV. It is clear that the use of the

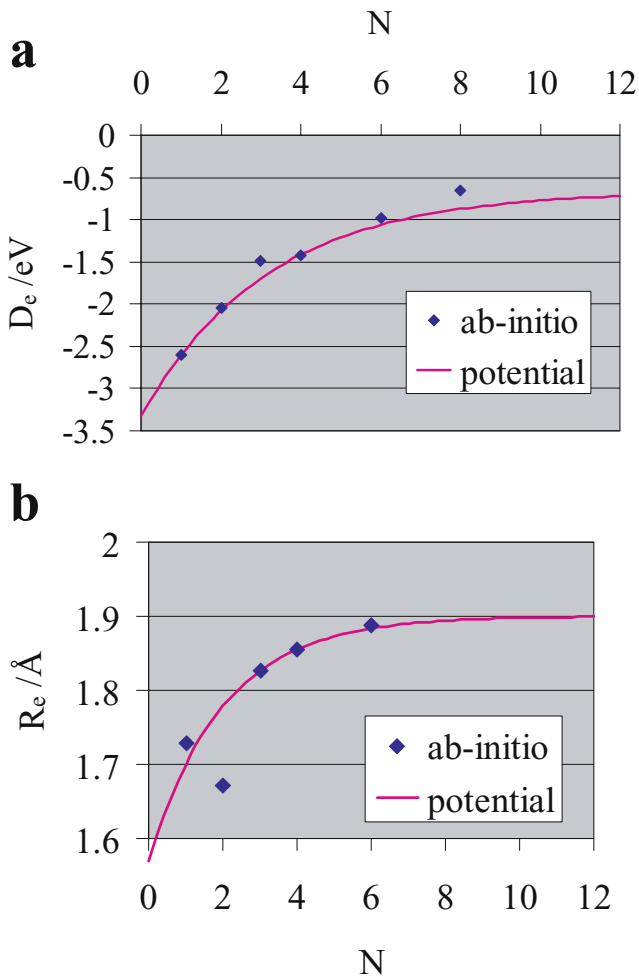


Fig. 4 a) Calculated binding energy (D_e , in eV) per C-Ni bond and b) C-Ni bond distance (R_e , in Å), as a function of the number of Ni atoms (N) in the clusters CNi_n

Table 2 Parameters for the weighting part of the C-C potential

N_1^M	N_2^M	R_1 (Å)	R_2 (Å)	R_1^M (Å)	R_2^M (Å)
3.5	6.0	2.7	3.0	1.8	2.8

original REBO potential for C atoms inside the metal cluster would overestimate the strength of such C-C interactions and would yield C structures inside the metal cluster that do not exist because of the screening of the C-C interaction by the surrounding metal atoms.

Equation (22) describes the transition of α_{1ij}^{TB} from 1.0 to 0.1 when N_{ij}^M (the average number of metal atoms surrounding the two C atoms involved in the C-C interaction) varies from an initial value, N_i^M , to a final value, N_2^M . N_i^M lies between 3 and 4 (3 is the coordination number of a C atom on the surface of the metal; a C atom with coordination number 4 is actually under the surface and has began to feel the screening of the metal atoms over the C-C interactions). N_2^M ranges between 6 and 8 (6 is the minimum coordination number of C in the bulk metal, 8 is the average coordination number inside a nanoparticle, according to our calculations).

α_{2ij}^{TB} is obtained from the geometric mean of α_{2i}^{TB} and α_{2j}^{TB} (each given by Eq. (28)). α_{2i}^{TB} describes the reactivity of C atoms ranging from $\alpha_{2i}^{TB} = 0.1$ for non reactive C atoms, to $\alpha_{2i}^{TB} = 1.0$ for reactive C atoms. Equation (28) describes the variation of α_{2i}^{TB} with decreasing R_i^M , the distance between the C atom i and its nearest metal atom. α_{2i}^{TB} becomes 1.0 when R_i^M is less than R_1^M (taken as the C-metal bond distance) and in that case the attractive part of the REBO potential is fully activated.

We emphasize that our simulation model for the nanotube growth assumes that the precursor atoms are catalyzed by the metal cluster producing C atoms, and that such reaction is irreversible. In terms of the force field, this means that when α_{2i}^{TB} is equal to 1.0 (i.e. the C atom is “catalyzed”) and remains at this value for the rest of the simulation independently of the value of R_i^M . R_2^M , the distance where the C atoms begin to catalyze is approximately the cutoff distance of the C-Metal potential. The actual parameters used in our simulations [21, 22] for Eqs. (21–28) are given in Table 2.

Results of molecular dynamics simulations using the reported metal-C and C-C potentials have been reported elsewhere [21, 22].

Conclusions

Interatomic metal-C and C-C potential functions containing the most important features of the interactions between such chemical species during the catalyzed synthesis of single-wall carbon nanotubes have been presented. Metal-C potential parameters obtained from DFT calculations are reported for the Ni-C system. With these potentials, the growth stages in the first steps of nanotube formation have been clearly identified [21, 22].

Acknowledgements Financial support from the National Science Foundation (NER/CTS-04003651) is gratefully acknowledged. This research used resources of the National Energy Research Scientific Computing Center, which is supported by the Office of Science of the U.S. Department of Energy under Contract No. DE-AC03-76SF00098. Supercomputer time granted by the DoD Major Shared Resource Center (ARL MSRC) is gratefully acknowledged.

References

- Iijima S, Ichihashi T (1993) Nature 363:603–605
- Rinzler AG, Liu J, Dai H, Nikolaev P, Huffman CB, Rodriguez-Macias FJ, Boul PJ, Lu AH, Heymann D, Colbert DT, Lee RS, Fischer JE, Rao AM, Eklund PC, Smalley RE (1998) Appl Phys A 67:29–37
- Journet C, Maser WK, Bernier P, Loiseau A, delaChapelle ML, Lefrant S, Deniard P, Lee R, Fischer JE (1997) Nature 388:756–758
- Peigney A, Laurent C, Dobigeon F, Rousset A (1997) J Mat Res 12:613–615
- Hafner JH, Bronikowski MJ, Azamian BR, Nikolaev P, Rinzler AG, Colbert DT, Smith KA, Smalley RE (1998) Chem Phys Lett 296:195–202
- Kitiyanan B, Alvarez WE, Harwell JH, Resasco DE (2000) Chem Phys Lett 317:497–503
- Li Y, Kim W, Zhang Y, Roland M, Wang D, Dai H (2001) J Phys Chem B 105:11424–11431
- Alvarez WE, Pompeo F, Herrera JE, Balzano L, Resasco DE (2002) Chem Mat 14:1853–1858
- Zhang L, Balzano L, Resasco DE (2005) J Phys Chem B 109:14375–14381
- Mann DJ, Halls MD, Hase WL (2002) J Phys Chem B 106:12418–12425
- Maruyama S, Shibuta Y (2002) Mol Cryst Liq Cryst 387:311–316
- Vinciguerra V, Buonocore F, Panzera G, Occhipinti L (2003) Nanotechnology 14:655–660
- Hernandez E, Ordejon P, Boustani I, Rubio A, Alonso JA (2000) J Chem Phys 113:3814–3821
- Bolton K, Rosen A (2002) Phys Chem Chem Phys 4:4481–4488
- Bernholc J, Rabec CB, Nardelli MB, Maiti A, Roland C, Yakobson BI (1998) Appl Phys A 67:39–46
- Shibuta Y, Maruyama S (2002) Physica B 323:187–189
- Roland C, Bernholc J, Brabec C, Nardelli MB, Maiti A (2000) Mol Simul 25:1–12
- Erkoc S, Malcioglu OB (2001) Int J Mod Phys C 12:865–870
- Ding F, Bolton K, Rosen A (2004) J Phys Chem B 108:17369–17377
- Raty J, Gygi F, Galli G (2005) Phys Rev Lett 95:096103
- Zhao J, Martinez-Limia A, Balbuena PB (2005) Nanotechnology 16:S575–S581
- Balbuena PB, Zhao J, Huang S, Wang Y, Sakulchaicharoen N, Resasco DE (2006) J Nanosci Nanotech 6:1247–1258
- Zhao J, Balbuena PB (2006) J Phys Chem A 110:2771–2775
- Brenner DW (1990) Phys Rev B 42:9458–9471
- Brenner DW, Shenderova OA, Harrison JA, Stuart S, Ni B, Sinnott SB (2002) J Phys Condens Matter 14:783–802
- Maiti A, Brabec CJ, Roland C, Bernholc J (1995) Physical Review B 52:14850
- Yamaguchi Y, Maruyama S (1999) Eur Phys J D 9:385–388
- Resasco DE, Alvarez WE, Pompeo F, Balzano L, Herrera JE, Kitiyanan B, Borgna A (2002) J Nanoparticle Res 4:131–136
- Fan X, Buczko R, Puretzky AA, Geohegan DB, Howe JY, Pantelides ST, Pennycook SJ (2003) Phys Rev Lett 90:Art. No. 145501
- Tersoff J (1989) Phys Rev B 39:5566–5568
- Numakura H, Kashiwazaki K, Yokohama H, Koiwa M (2000) J Alloys Compd 310:344–350